

Plasma Bulk Flow in Jupiter's Dayside Middle Magnetosphere

MARK R. SANDS¹

Department of Nuclear Engineering and Center for Space Research, Massachusetts Institute of Technology, Cambridge

RALPH L. MCNUTT, JR.

Department of Physics and Center for Space Research, Massachusetts Institute of Technology, Cambridge

Using the plasma data obtained during the Voyager 1 encounter and the full response function of the Plasma Science (PLS) experiment, convective plasma velocities have been determined in the dayside middle magnetosphere of Jupiter ($10 R_J < r < 25 R_J$). We find that temperature anisotropies have very little effect on plasma velocity determination and that the plasma data are well approximated by convected, isotropic Maxwellian ion distribution functions. The insensitivity of the analysis to any thermal anisotropies which may exist allows a good determination of the bulk plasma flow velocity. In addition to the subcorotational azimuthal flow there exists a substantial nonazimuthal component of plasma flow. This nonazimuthal flow is mostly aligned (antialigned) with the local magnetic field but also exhibits a cross-field component. The velocity pattern is inconsistent with enhanced plasma outflow in the active sector, as suggested by the corotating convection model of plasma transport. The contribution of field-aligned flow along the curved magnetic field lines to the stress on the magnetic field is evaluated. In the region studied such flow contributes up to one half the stress produced by the azimuthal plasma flow.

INTRODUCTION

Pioneer Observations

From observations with the Pioneer spacecraft, *Smith et al.* [1975] found that Jupiter's magnetic field does not lie in meridional planes but instead exhibits a spiral structure. An explanation of this observation was put forward by *Northrop et al.* [1974]: slippage of magnetic field lines with respect to the planet implying that the plasma motion deviates from rigid corotation. *McDonald et al.* [1979] found from particle anisotropies measured by Pioneer 10 that outside of $45 R_J$ ($1 R_J \equiv 71,398$ km), energetic protons (0.5 – 2.15 MeV) exhibited anisotropies inconsistent with rigid corotation.

In addition to partial corotation, plasma streaming along magnetic field lines was observed in the middle magnetosphere of Jupiter [*Van Allen et al.*, 1974; *McDonald et al.*, 1979; *Northrop et al.*, 1979]. In looking at the energetic proton (0.2 – 20 MeV) data from Pioneers 10 and 11, *McDonald et al.* [1979] found large anisotropies which they determined were due both to the effects of partial corotation and the effects of magnetic-field-aligned streaming. A much smaller anisotropy was apparently due to spatial gradients in particle intensity. A detailed analysis of 1.8- to 2.15-MeV proton data taken by Pioneer 10 was performed by *Northrop et al.* [1979]. In one case they assumed that the ion distribution function f_0 was isotropic, allowed no field-aligned flow, and assumed the electric field to be due entirely to corotation. In a second case, f_0 was allowed to be anisotropic, and finally, in a third case, f_0 was again assumed isotropic, but parallel flow was allowed. The only case which was able to account for most of the anisotropy was that which assumed parallel flow. The other cases required density gradients which were orders of magnitude too large (and sometimes in the wrong direction), while almost no gradient was needed if field-

aligned flow was assumed. Both this analysis and the analysis of *McDonald et al.* [1979] suggest that at least a part of this field-aligned flow is directed away from the magnetic equator. Consequences of such flows for particles at these large energies are discussed by *Northrop* [1979] and *Northrop and Schardt* [1980].

Voyager Observations

Following the Jupiter flybys with the Voyager 1 and 2 spacecraft, plasma flow in the dayside middle magnetosphere has become better understood. Initial results from both encounters confirmed that the plasma moves primarily in the corotational (azimuthal) direction. However, outside of $\sim 10 R_J$ the data from the Plasma Science (PLS) experiment indicates that the azimuthal component of velocity becomes almost constant, i.e., the plasma does not rigidly corotate with the planet [*Bridge et al.*, 1979b; *McNutt et al.*, 1979; *Belcher et al.*, 1980; *McNutt et al.*, 1981]. In addition to the subcorotational flow, *Belcher and McNutt* [1980] and *McNutt et al.* [1981] qualitatively showed that plasma flowed away from the magnetic equator on the dayside and toward the equator on the nightside during the Voyager flybys. These observations are consistent with inferences of *Northrop et al.* [1979] and *McDonald et al.* [1979] regarding the motion of higher-energy particles. At that time no quantitative information on the magnitude of these flows was readily available.

Anisotropy measurements at high particle energies by the Low Energy Charged Particle (LECP) experiment suggest that the true situation may be even more complicated. *Carbary et al.* [1981] interpreted first-order particle flux anisotropies in the 0.57- to 1.78-MeV proton channel as being due to bulk flow of the plasma (Compton-Getting effect) and derived both speed and direction (in the LECP scan plane) of plasma bulk flow. Their results are in good agreement with the PLS results in locations where good determinations are available from both experiments. In particular, *Carbary et al.* [1981] confirm the observation of subcorotational flow within $\sim 20 R_J$ of Jupiter and in the crossings of the cold plasma sheet along the inbound leg of the Voyager 1 trajectory (within $\sim 45 R_J$ of the planet). Outside of $\sim 20 R_J$ and away from the cold plasma locations, unambiguous velocity component determinations at all locations are not possible using the PLS data

¹Now at Science Applications International Corporation, McLean, Virginia.

alone. *Carbary et al.* [1981] find anisotropy amplitudes indicative of corotation when the anisotropy direction is consistent with corotation. These conditions occurred along the Voyager 1 inbound trajectory four times between the last inbound magnetopause crossing and $\sim 25 R_J$ (refer to their Figure 18). At times of nonazimuthal flow, as determined by the first-order anisotropy direction, the flow tends to be in the sunward direction (as projected into the LECP scan plane), but there is a great deal of scatter in the direction. The Voyager 1 anisotropy amplitudes also show a ~ 10 -hour periodicity.

The situation at the time of the Voyager 2 encounter is even less clear. Plasma velocities determined from PLS data acquired between ~ 10 and $17 R_J$ inbound are sometimes significantly below corotation and exhibit fairly large field-aligned (antialigned) components [McNutt *et al.*, 1987]. A single spectrum obtained further out ($\sim 22 R_J$) also shows a smaller velocity component into the PLS side sensor than would be expected on the basis of rigid corotation [Bridge *et al.*, 1979b]. First-order anisotropy measurements from the LECP experiment were only available in to $\sim 30 R_J$. Both the amplitudes and directions are consistent with azimuthal flow at less than rigid corotation speed on average but with a great deal of scatter (see Figure 19 of *Carbary et al.* [1981]). Outbound from Jupiter, viewing geometries for both the PLS and LECP instruments usually were not favorable for determining bulk flow velocities or any of their components.

As long as the ionosphere of Jupiter is not a perfect conductor and plasma is flowing away from the planet, there is a distance beyond which the torque provided by the ionosphere is insufficient to impart enough angular momentum to the plasma to keep it corotating with the planet [Hill, 1979; Vasyliunas, 1983]. The Voyager 1 PLS observations of deviations from corotation are consistent with inferred ionospheric conductivities and plasma production rates at Io [Hill, 1980].

There has been speculation about whether the LECP data from the Voyager 1 encounter are also consistent with this picture, considering the apparent "speeding up" of the plasma to rigid corotation speed at large distances from the planet. It is possible that the variations inferred from the LECP anisotropies are due to time-dependent variations driven by changing solar wind parameters [McNutt *et al.*, 1987] although this is unlikely given the periodicities noted in the inferred flow speed. Other treatments of the LECP data have tended to confirm the results noted above [Brown *et al.*, 1985; Paonessa, 1985], although the details are sketchy. The variations noted by *Carbary et al.* [1981] could also be consistent with the "inertial breakdown model" if the points exhibiting rigid corotation occur at the magnetic equator, while other points exhibiting more deviation correspond to field lines crossing the magnetic equator at much larger distances from the planet, due to the distension of the field lines by the Jovian current sheet (C. K. Goertz, private communication). Why the PLS data corresponding to relatively cold plasma occur at locations of intermediate values of the anisotropy-determined speed is not explained by such a scenario, however. Further study incorporating detailed comparisons of flow parameters determined from the PLS and LECP data will be required to determine whether there is an observational versus theoretical controversy, and, if so, its resolution. Such a study will involve the detailed idiosyncracies of both instruments and their respective data sets; it is beyond the scope of this paper.

Current Study

The main result of the present analysis of the plasma data obtained by Voyager 1 in the dayside middle magnetosphere is a

more quantitative look at the plasma flow. Previous studies in this region using the PLS data determined only one component of the convective velocity (primarily the azimuthal component, see, e.g., *McNutt et al.* [1981]). This study applies the techniques used by *Barnett and [1986]* in analyzing data obtained during the Io flux tube flyby to data obtained during the dayside pass of Voyager 1. Although we find most of the flow to be in the azimuthal direction (and subcorotational), the flow component away from the magnetic equator can have a magnitude in excess of 35% of the corresponding azimuthal flow component. The cross-field flow component in the dayside middle magnetosphere is typically ≤ 15 km/s in magnitude.

Analysis of the plasma data was confined to the dayside middle magnetosphere owing to spacecraft orientation and an effect of plasma "temperature." With respect to orientation, on the inbound leg of the trajectory azimuthal flow is seen primarily by the D cup, and any nonazimuthal flow is reflected in the B and C cup data. Outbound, the spacecraft was oriented so that the D cup pointed northward of the equatorial plane and the symmetry axis of the main sensor pointed earthward and well away from the direction for viewing corotating plasma. The various cups exhibit currents above the noise level in this region, and a determination of plasma flow during the outbound pass may be possible with more work. However, the viewing geometry makes such an analysis much more difficult than that presented here and lies beyond the scope of this effort.

With respect to "temperature," a spectrum is considered "hot" when the thermal velocity is large enough to yield an effective Mach number M roughly less than 5 (we define effective Mach number as the ratio of the bulk flow into a particular cup to the thermal speed for a given ionic component). In this case, the individual heavy ion peaks making up a spectrum begin to overlap, and, if the spectrum is hot enough, only one large broad peak is present (the proton peak remains resolved to lower values of M). Such data cannot necessarily be analyzed in a unique fashion (the extent to which the parameter determinations are unique is even difficult to assess in this case). However, if $M > 5$, the individual ion peaks are distinguishable, and unique plasma parameters can easily be determined.

INSTRUMENT

The Plasma Science (PLS) experiment on the Voyager 1 and Voyager 2 spacecraft consists of two plasma detectors. One detector, the main sensor, is made up of three modulated-grid Faraday cups, the A, B, and C cups, while the side sensor, or D cup, consists of one modulated-grid Faraday cup. The symmetry axis of the main sensor is parallel to the axis of the high-gain antenna on the spacecraft and thus points toward the Earth, except for short periods of time during some spacecraft maneuvers. The normals of the three cups of the main sensor are tilted $\sim 20^\circ$ to the symmetry axis and are equally spaced $\sim 120^\circ$ in azimuth about that axis. The D cup normal is $\sim 88^\circ$ to the symmetry axis and is located 167° in azimuth from the A cup normal.

Currents due to positive ions are measured simultaneously by all four cups in the energy-per-charge range of 10 – 5950 V. In addition, the side sensor measures currents due to electrons over the same energy-per-charge range. This range is covered by a set of discrete, contiguous voltage windows which, to first order, are spaced logarithmically. While measuring positive ions, there are two instrument modes which can be utilized. The low resolution mode (L mode) breaks up the energy range into 16 voltage windows, each with an energy-per-charge resolution ($\Delta E/E$) of $\sim 29\%$; the high-resolution mode (M mode) has 128 voltage windows, each with an energy-per-charge resolution of $\sim 3.6\%$.

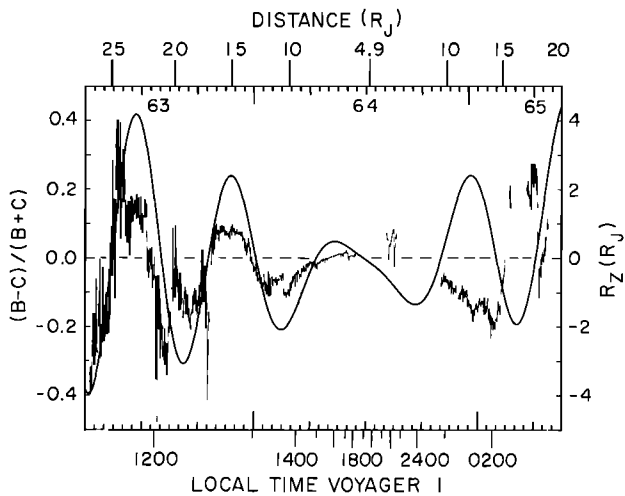


Fig. 1. Plot of the difference between the B and C cup flux densities divided by their sum from the Voyager 1 encounter with Jupiter. Superimposed on this plot is the distance of Voyager 1 from the plane of the magnetic equator. The same variation in the observed ion fluxes as a function of spacecraft magnetic latitude was found during the Voyager 2 encounter half a year later. Reprinted from *McNutt et al.* [1981].

During the encounters with Jupiter and Saturn a complete L mode takes 3.84 s to acquire, while a complete M mode measurement takes 30.72 s. Each measurement sequence lasts 96 s, during which currents from either the first or last 72 energy channels of the M mode are telemetered to Earth. Thus a complete M mode spectral set is received at Earth every two measurement sequences, i.e., in 192 s. The convention adopted here for analysis of M modes involves producing one entire set of M mode spectra (from all four cups) every 192 s by combining channels 1 – 56 from one measurement sequence with channels 57 – 128 from the subsequent sequence. A more detailed description of the PLS experiment is given by *Bridge et al.* [1977].

ANALYSIS TECHNIQUE

Once received, data from the PLS experiment during the Voyager 1 and 2 encounters with Jupiter can be analyzed to determine composition, density, velocity, and other properties of the plasma. Analysis of the data consists of trying to duplicate the currents measured by the PLS experiment with currents calculated using an analysis program given assumed constraints. This analysis routine allows the user to choose a model for the calculated currents and then proceeds through a nonlinear least squares fitting routine to try to match calculated currents with measured currents. The algorithm used is that due to Marquardt [*Bevington, 1969*].

Even though many spectra can be analyzed assuming the plasma distribution functions are convected isotropic Maxwellians, there are spectra which cannot be duplicated (i.e., fit) using this assumption. For example, by assuming ion distributions to be isotropic Maxwellians, temperature (pressure) anisotropies cannot be taken into account. To investigate the possibility of temperature anisotropies and their effect on fits to the data, we modified and expanded upon the algorithm developed to analyze the Io flux tube data [*Barnett, 1984; Barnett and Olbert, 1986*] to incorporate the response of the PLS detectors to bimaxwellian distributions. Details of the algorithm are given by *Sands [1987]*; a summary is included in the appendix.

In all, 44 spectral sets were selected for analysis. Four of these were subjected to slightly different initial guesses of the fit parameters to verify the insensitivity of the final results to the initial guesses in the nonlinear fitting procedure. Of the 44 sets, 11 were from the PLS L mode and 33 from the M mode. In the cases that L mode sets were used, adjacent M mode spectra from the D cup were used to determine initial guesses for the densities and thermal speeds. In these cases, the currents in the B and C cups of the M mode were near the noise level, so the L mode spectra, with their higher signal-to-noise ratio, had to be used to determine the flow velocities. Details are given by *Sands [1987]*.

MAXWELLIAN FITS

An indication of plasma flow can be found from considering the total particle flux into the various PLS cups [*Belcher and McNutt, 1980*]. For example, during the period of interest the currents measured in the B and C cups are not the same. In Figure 1 the fractional difference in these currents (left vertical scale) is plotted against spacecraft event time (SCET). The distance indicated at the top of the plot is the radial distance from the center of the planet, measured in terms of R_J . Superimposed on this plot is the location of Voyager 1 with respect to the magnetic equatorial plane. Local time is shown on the bottom scale. If one assumes the ion distribution functions are convected Maxwellians, the differences in flux densities can only be accounted for by a non-azimuthal bulk plasma flow. However, these differences could also be due to non-Maxwellian features, a possibility we discuss in the next section.

Assuming the distribution functions of the various ion species are well approximated by convected isotropic Maxwellian distributions, the spectral data can be analyzed in a manner similar to the data from the Io flux tube passage [*Barnett, 1986*]. One positive ion spectrum from this period which has been analyzed this way is shown in Figure 2; it was obtained by Voyager 1 on March 4 at 2323 SCET. The spacecraft was approximately 13.5 R_J from the magnetic dipole axis of Jupiter and 1.06 R_J above the magnetic equator. The labels A, B, C, and D refer to the four cups of the PLS experiment. Currents are measured in units of femtoamperes (10^{-15} ampere = 1 femtoampere) on the vertical axis, while channel number on the horizontal axis refers to the energy-per-charge channels discussed above.

The ions in the spectra are quite "cold;" i.e., three peaks representing the heavy positive ions can be picked out as well as the proton peak. Five positive ion species were assumed (H^+ , O^{+2} , S^{+3} , O^+ (S^{+2}), and S^+) in the analysis; the fit parameters include the three components of the convective velocity (assumed the same for all of the various ionic species) V_R , V_ϕ , and V_z , and the five ion densities. The components of velocity are referred to a set of cylindrical coordinates in which the z axis is aligned with the spin axis of Jupiter. The proton thermal speed was also a fit parameter with the other four ion thermal speeds determined from the proton thermal speed, assuming a common temperature. Results of the fit are shown in Figure 3. All the peaks in the D cup are fit quite well, as are the lower energy channels in the B and C cups. We note that the assumption of a common temperature for the ions produces a good fit to the measured currents in the D cup in which the various peaks are resolved. This same assumption has been applied throughout the analysis presented here in order to (1) introduce some constraint in the fits and (2) limit the required amount of computer time for doing the analysis. While we have not done a complete mapping of the consequences of this assumption in the corresponding fit

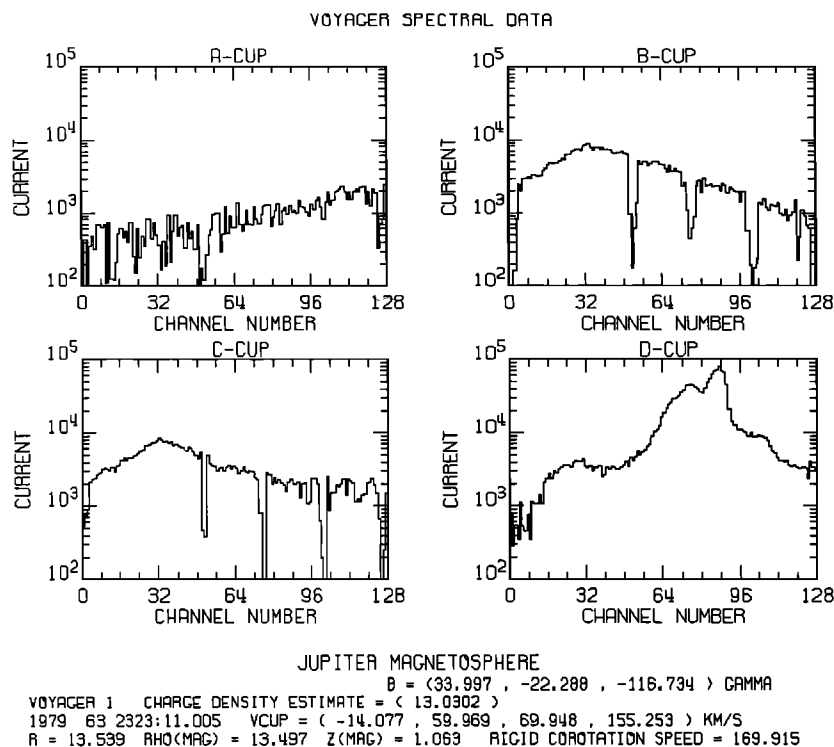


Fig. 2. Spectra obtained by Voyager 1 on March 4 at 2323 SCET. The spacecraft was approximately $13.5 R_J$ from the dipole axis and $1.06 R_J$ above the magnetic equator. All the ion peaks are well resolved in the D cup allowing an unambiguous determination of the thermal component of the plasma.

parameter space, we have done cross checks on some spectra which indicate (1) that this is actually a good assumption and (2) that the velocity determinations are insensitive to this assumption. We have also been conservative in our selection of spectra to fit; i.e., we only used spectra in which there was at least a partial resolution of the heavy ion peaks in the D cup. This approach allowed us to verify that the common temperature assumption did indeed produce good fits to the data. Further work on the effect of such assumptions on less well resolved spectra than those used in this study is in progress.

The signal present in the upper channels of the B and C cups and in the A cup may be due to a hot ion background; it is also present in the currents in the D cup at high energies and between the proton and heavy ion signatures. This background ion population was not fit for two reasons: First, it does not significantly affect the velocity calculation, and second, it is very hard numerically to take this hot ion background into account, as its composition and distribution functions are not known a priori. It is also possible that some of this signal may be due to contamination by the hot electron population present at this time. Such contamination is similar to that of the ions on the electron measurements obtained in the warm Io plasma torus (see the appendix of *Sittler and Strobel* [1987]). A full discussion of this effect is complex and beyond the scope of this paper. Regardless of which of these is the source of the currents in the higher channels, we expect them to produce currents that increase with increasing energy-per-charge and to contribute about equally to all cups. Given that the peak currents in the B, C, and D cups (which contribute the most to the determination of the flow velocity) are above the measured current levels in the highest channels, simply neither including the latter currents in the fits

(only the lower energy-per-charge channels were used in the B and C cups, although the exact channels used varied from spectrum to spectrum) nor "subtracting" them out (their actual contribution to the lower energy channels is not known) should still result in a good velocity determination. This is the most conservative approach known at this time which can be used in this type of analysis. The signature in the upper channels is the subject of an ongoing study; we do not anticipate a better understanding of the origin of these currents to change the analysis results presented here, however.

Analysis of the spectral set shown in Figure 3 yields a bulk plasma flow of $V = -4.5 \hat{e}_R + 139.7 \hat{e}_\theta + 16.7 \hat{e}_z$ km/s (again referred to a Jovicentric cylindrical coordinate system). Velocities obtained through the analysis of similar spectra from this region are shown in Figure 4, where each velocity component (in km/s) is plotted against spacecraft event time (cylindrical radial distance from the magnetic dipole axis is shown across the top). There are two major results. First is the reconfirmation (using the full response function of the PLS instrument) that the plasma departs from strict corotation about Jupiter as one moves out from the planet. *McNutt et al.* [1981] originally noted that the plasma starts to depart from corotation at least as close as $\sim 10 R_J$ to Jupiter, but that analysis used only D cup spectra from which a velocity component normal to the D cup was obtained and shown to be inconsistent with the rigid corotation of the plasma. Utilizing the full response function to derive the full convective velocity vector leads to the second major result that there is a substantial nonazimuthal plasma flow component. Again we note that this feature had been shown to exist qualitatively [*Belcher and McNutt*, 1980; *McNutt et al.*, 1981], but the magnitude remained unknown. The observed velocities of

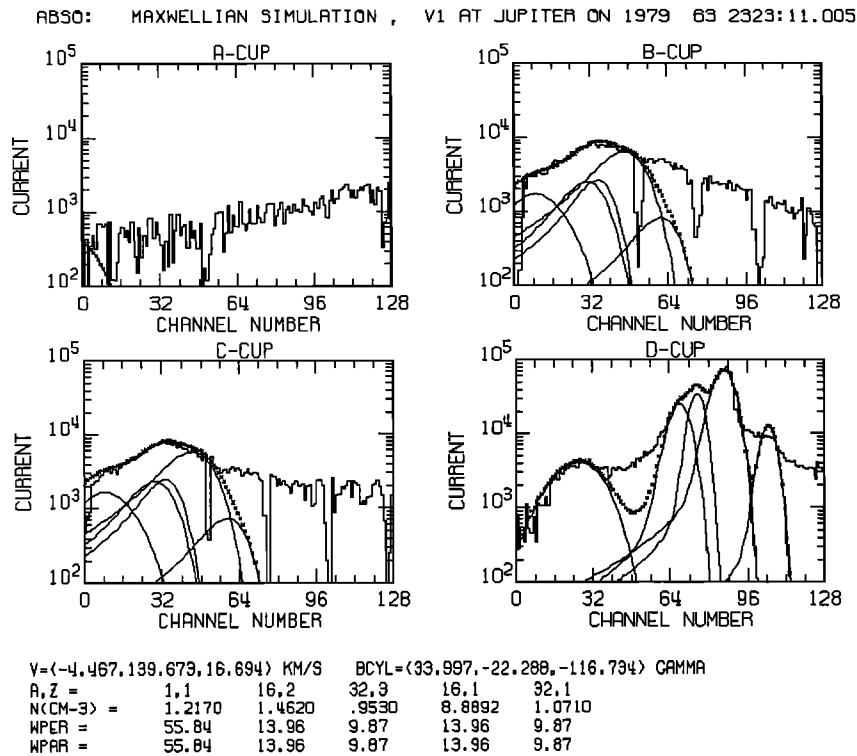


Fig. 3. Currents calculated for the spectra of Figure 2, assuming that the ion distribution functions are convected isotropic Maxwellians. The simulated currents are superposed on the spectral data for easy comparison. Calculated currents due to each ion species are shown by the individual peaks. Fit parameters are shown in the lower panel (velocity and thermal speed in kilometers/second, densities in number/cubic centimeter).

up to ~ 50 km/s (20.5 km/s = $1 R_J/h$) suggest that this flow cannot be ignored in considering magnetospheric dynamics.

Instead of using a Jovicentric cylindrical coordinate system, the magnetic field (obtained from the Voyager magnetometer) and the plasma bulk flow velocities can be transformed to a tilted dipole cylindrical coordinate system (based upon the dipole axis tilted 9.6° to the rotation axis and pointing toward the system III longitude of $\lambda_{III} = 201.7^\circ$, the dipole from the O_4 magnetic field model [Acuña *et al.*, 1983]). With the velocities and magnetic field given in this system, it is easier to visualize how much of the nonazimuthal flow is field-aligned and how much is cross-field flow. To make certain only the effect of the nonazimuthal flow is seen, a frame of reference which moves with the azimuthal flow component (i.e., in which $V_\phi = 0$) is chosen. Using the radial and axial components of the parallel and perpendicular flows (i.e., $V_{\parallel R}, V_{\perp R}, V_{\parallel Z}, V_{\perp Z}$) and the radial and axial components of B , we constructed Figure 5. The wavy line is a projection of the Voyager 1 spacecraft's trajectory onto magnetic meridional planes, with ZMAG being the distance above or below the magnetic equator and RMAG the cylindrical distance from the dipole axis; both distances are in units of Jovian radii. The poloidal (nonazimuthal) component of the magnetic field for each spectrum is represented by the dashed arrows. Solid arrows represent the nonazimuthal component of the bulk plasma flow obtained for each plasma spectral set. There are several important features of Figure 5 to note.

An important feature is the size of the field-aligned (antialigned) portion of the flow. Every spectral set analyzed gives a flow which yields a significant field-aligned (antialigned)

component. The magnitude of this component ranges from about half to all of the magnitude of the total nonazimuthal flow.

A second point made in Figure 5 concerns the direction of flow. From $\sim 13 R_J$ to $18 R_J$ the flow is consistently away from the magnetic equator. Two spectral sets analyzed in the vicinity of $20 R_J$ and one at $\sim 25 R_J$ also follow this trend (the analysis results from $\sim 25 R_J$ are indicated on Figure 4 but not on Figure 5). Generally unfavorable viewing geometry and lack of resolved peaks and constraints on available computation time precluded a more detailed analysis in the region between $25 R_J$ and $18 R_J$, although the spectra in this region are qualitatively similar to those three sets subjected to analysis. For the analyzed spectral sets we found that when the spacecraft is above (north of) the equator, flow is to the north and when below the magnetic equator, observed flow is in the southern direction. The similarity with the pattern in Figure 1 is obvious. However, inside of $13 R_J$ the flow is still toward the north and hence toward the equator, even though the spacecraft is at southern magnetic latitudes. The slight upward deviation at this time in the relative flux shown in Figure 1 may reflect this change in the flow pattern, although it emphasizes the difficulty in trying to derive a sense of the flow from the data shown in Figure 1 alone.

The cross-field component of the flow also exhibits peculiarities. From approximately $15 R_J$ to $25 R_J$ the cross-field flow is away from Jupiter, while between $11 R_J$ and $13 R_J$ the flow is toward the planet. In the range $13 R_J$ to $15 R_J$ the cross-field flow is very small and oscillates back and forth away from Jupiter and inward toward the planet.

The magnitudes of the field-aligned and cross-field components

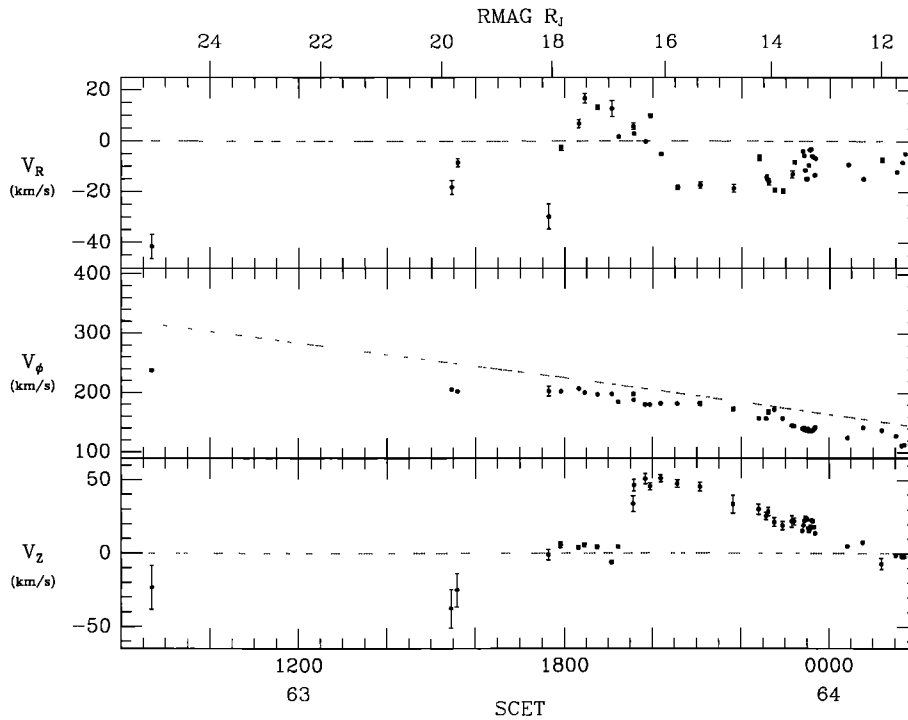


Fig. 4. Plasma bulk flow velocities (in cylindrical coordinates), obtained through the analysis plotted against spacecraft event time. The dotted line in the plot of azimuthal velocity, V_ϕ , represents the local rigid corotational velocity, while those in the plots of V_R and V_z represent zero velocity component. The error bars indicate the formal 1σ errors in these parameters. The cylindrical radial distance from the dipole axis RMAG is shown across the top in units of Jovian radii; spacing between the distance markers varies owing to the spacecraft speed and the wobbling motion of the magnetic axis.

are comparable to those found by *McNutt et al.* [1987] for the Voyager 2 encounter. The region investigated for the Voyager 2 encounter ($10.1 R_J$ to $16.7 R_J$) is similar to that studied here, but that analysis was less detailed and was performed on fewer spectra owing to limitations of the data.

BIMAXWELLIAN FITS

Although our simulations of the data indicate that the suprathermal ions (and/or electron contamination) should not affect the determination of the convective velocity for the spectra

fit, it is not clear a priori what would be the effect of a thermal anisotropy on the other fit parameters.

To determine whether the deduced nonazimuthal component of plasma flow is, in reality, a manifestation of a thermal anisotropy, selected spectra were reanalyzed, allowing parallel and perpendicular thermal speeds to vary independently. One of these reanalyzed sets of spectra is that one shown in Figure 1 (the Maxwellian simulation to this set was presented in the previous section).

In this analysis, the simulation algorithm outlined in the

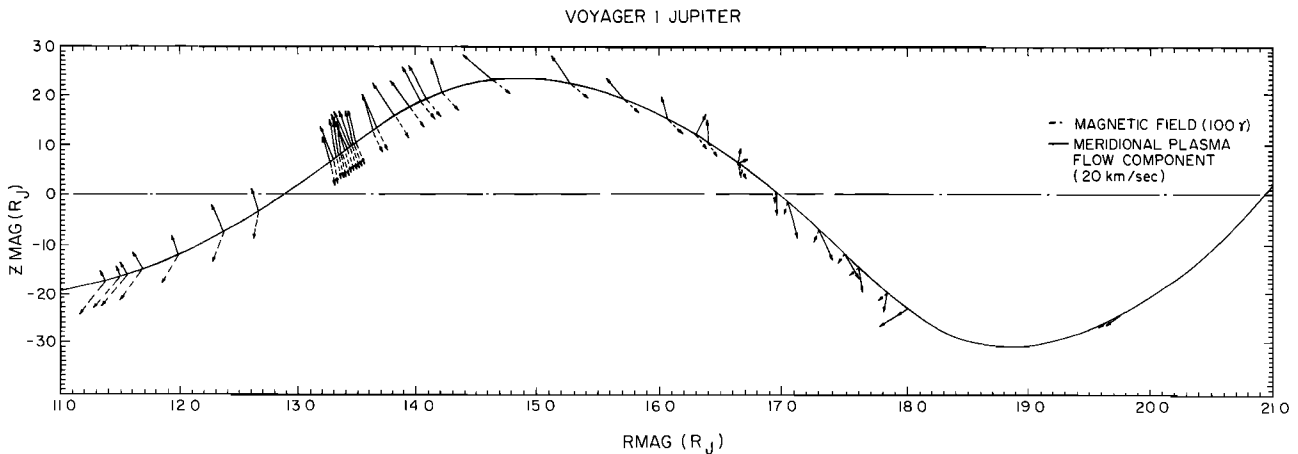


Fig. 5. A vector plot of the calculated nonazimuthal component of the plasma bulk flow and associated magnetic field. A tilted dipole coordinate system is used, where ZMAG is the distance the spacecraft is above or below the magnetic equator and RMAG the cylindrical radial distance from the dipole axis. The placement of the vectors corresponds to the spacecraft location at the times of the associated spectra. Magnetic field is represented by the dashed arrows, while the solid arrows indicate the nonazimuthal bulk plasma flow.

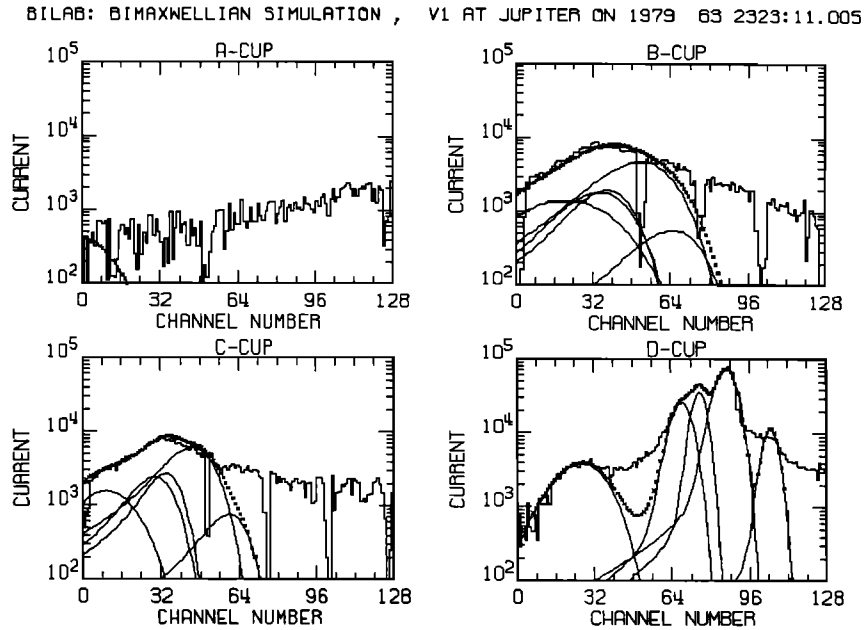


Fig. 6. Result of a fit, assuming the ion distribution functions are bimaxwellian, to the spectral set shown in Figure 2. There is very little difference between this fit and the fit assuming convected isotropic Maxwellian ion distribution functions. Total and individual ion currents are superposed on the spectra. The corresponding fit parameters are, for H^+ , O^{++} , S^{+++} , $O^+(S^{++})$, and S^+ , density (cm^{-3}): 1.63, 1.39, 0.91, 8.34, and 0.93; perpendicular thermal speed (km/s): 56.89, 13.59, 9.61, 13.59, and 9.61; parallel thermal speed (km/s): 190.97, 40.87, 28.9, 40.87, and 28.9, respectively.

appendix was employed. The same fit parameters as in the Maxwellian case were used, but now the proton parallel and perpendicular thermal speeds are allowed to vary independently and are fit independently of the heavy ions, which are assumed to have common values of T_{\parallel} and T_{\perp} . This choice was made to limit the number of fit parameters while still allowing for an assessment of the effect of an anisotropy in the plasma. Results of this fit are shown in Figure 6. The fit currents, assuming a convected bimaxwellian, are practically identical to those obtained in the convected Maxwellian fit. The only differences show up in the last few channels of the B cup and as a slightly larger signal in the A cup. Other spectra analyzed, assuming both a Maxwellian and a bimaxwellian ion distribution function, yield similar results. This example is shown because it exhibits the largest deviation between the two cases and thus provides an upper limit to anisotropies in the thermal plasma in the region investigated. Because the hot ion background was not simulated, the effect of the fitting procedure is to increase the parallel temperature to account for the signal in the upper channels of the B and C cups. However, owing to the orientation of the cups, the current calculated in the A cup serves as a check on the maximum anisotropy allowed. A further increase in T_{\parallel} causes the calculated current in the A cup to overshoot the actual measured values, thus limiting the anisotropy. This "simulated" anisotropy gives an upper limit of the ratio $T_{\parallel}/T_{\perp} = 9.0$ for the heavy ions (here the thermal speeds for the protons, fit separately, yielded a higher ratio of 11.3). An important point to note is that the formal errors in w_{\perp} are small, $\sim 1.8\%$, while those in w_{\parallel} are large, $\sim 14\%$ (1-sigma level; formal errors in the proton fits are higher). The computed value for T_{\parallel}/T_{\perp} ranges between 12.1 and 6.5 at the 1-sigma level. At the same time, the calculated bulk plasma flow was practically identical to that found in the Maxwellian case; for the convected bimaxwellian distribution we obtained a convective

velocity of $V = -4.8 \hat{e}_R + 140.1 \hat{e}_{\phi} + 16.9 \hat{e}_z$ km/s. These values can be compared with those from the isotropic Maxwellian fit shown in Figure 3 for which $V = -4.5 \hat{e}_R + 139.7 \hat{e}_{\phi} + 16.7 \hat{e}_z$ km/s. The differences in these two sets of components are within the 1-sigma formal errors for the fits.

This result is typical. The orientation of the cup normals with respect to the magnetic field is such that for most of the encounter period the distribution functions are being "sliced" mostly perpendicular to the magnetic field. As a consequence, both the convective velocity and w_{\perp} are well determined if the ion convective flow into at least one of the cups is large in comparison to the thermal width to which the cup is sensitive. As this unambiguously fixes one velocity component, a combination of the thermal speeds (mostly w_{\perp}) and the densities, the allowed variation in the other velocity components with respect to the measured currents in the other cups is severely constrained. The spectral sets fit were selected to take advantage of these constraints so as to yield a good determination of the convective velocity vector.

Of all the spectra sent back by Voyagers 1 and 2 during the Jupiter encounters, only one spectral set to date has been identified as possibly exhibiting a true temperature anisotropy in an unambiguous way. The spectral set shown in Figure 7 was obtained by Voyager 2 on July 9, 1979, at 0720 SCET with the spacecraft $14.9 R_J$ from the dipole axis and $2.9 R_J$ below the magnetic equator (in the region of the plasma "voids;" see McNutt *et al.* [1987]). Because the spectra are so hot, the individual peaks of the heavy ions all merge into one broad peak. The proton peak, however, is still discernible in all four cups and can thus be used to yield a bulk plasma flow. Fit parameters consisted of the proton density, thermal speed, and all three components of the bulk plasma flow. All four cups were used in the analysis, as the proton signature is easily discernible in each cup. The best fit

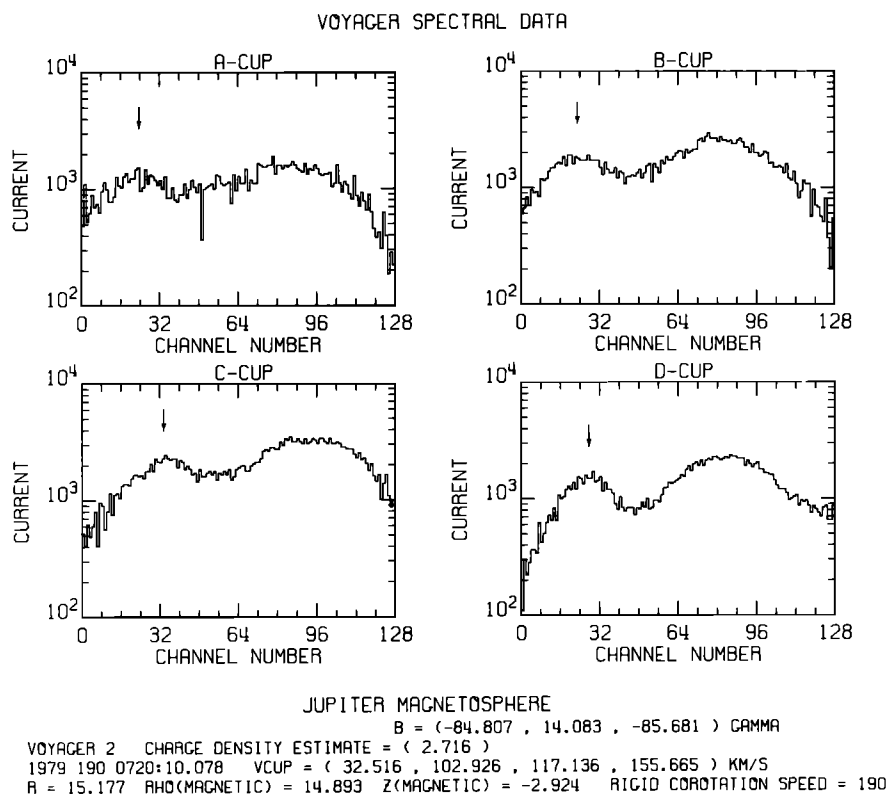


Fig. 7. A spectral set obtained on the inbound portion of the Voyager 2 encounter with Jupiter. Voyager is about $14.9 R_J$ from the dipole axis and $2.9 R_J$ below the magnetic equator. Because the plasma temperature is high, only the proton peak is resolved in the four cups (indicated by the arrows). Reprint from McNutt *et al.* [1987].

from the analysis, assuming a convected Maxwellian ion distribution, cannot simulate the currents corresponding to the proton peak in all four cups simultaneously. Results of this fit are shown in Figure 8. This inability to fit the signatures in all of the cups suggests that a convected bimaxwellian distribution might yield a better description of the data. Using the same fit parameters as before but now allowing the parallel and perpendicular thermal speeds to vary independently gives the fit shown in Figure 9. Allowing the parallel and perpendicular temperatures to float independently greatly improves the fit in all four cups and gives an anisotropy of $T_{\parallel}/T_{\perp} = 3.08 \pm 0.4$. The bulk velocity is $\mathbf{V} = -44.2 \hat{e}_r + 151.4 \hat{e}_\theta - 48.1 \hat{e}_z$ km/s, which includes a nonazimuthal component of flow much larger than in the Maxwellian case. However, the formal errors are much larger in the former case, reflecting the obviously "bad" fit to the spectra.

It is important to note that another explanation of this signature could be an isotropic Maxwellian combined with a negative spacecraft potential accelerating ions into all four cups. From the position of the proton peak in the A cup a potential of less than 100 V in magnitude may be capable of producing the signature, but full consideration of this possibility is beyond the scope of this paper.

Two important results follow from the bimaxwellian analysis: (1) the thermal components of the magnetospheric plasma are well approximated assuming a convected, isotropic Maxwellian distribution for the ions, and (2) the nonazimuthal flows obtained using a Maxwellian distribution are real and are accurately determined. As a final note, for the spectra of Figure 7 the nonazimuthal flow component occurs along with the anisotropy,

i.e., the determination of the flow velocity is decoupled from thermal anisotropy in the distribution function.

DISCUSSION

Flow Directions

Most of the nonazimuthal velocity is field aligned. The most notable exceptions to this are exhibited by the spectra from early on day 64 and the spectra during hour 18 on day 63. But even these spectra generally show a V_{\parallel} component which is greater than the V_{\perp} component. Except for the magnetic equator crossing just before day 64, the sign change on the parallel velocity component seems to be a good indicator of the spacecraft crossing the magnetic equator. As noted above, prior to the crossing of the magnetic equatorial plane near $\sim 13 R_J$ we find that when Voyager is above the magnetic equator, the flow is anti-field-aligned, i.e., toward the north magnetic pole, and, while below the magnetic equator, the observed flow is field aligned. This trend does not hold within $\sim 13 R_J$ but does hold for the isolated point near $25 R_J$. The magnitude of the parallel flow component is shown in Figure 10; the component of plasma flow along the magnetic field is plotted versus the total nonazimuthal flow. For reference, a dotted line has been drawn representing the locus of points where the magnitude of V_{\parallel} equals the magnitude of the total nonazimuthal plasma velocity. The magnitude of this nonazimuthal flow reaches almost 50 km/s, which translates to approximately $2.5 R_J/h$. The isolated point near $25 R_J$ (not shown) exhibits a parallel velocity component of 68 km/s and a total nonazimuthal component of 74 km/s. It is interesting to note

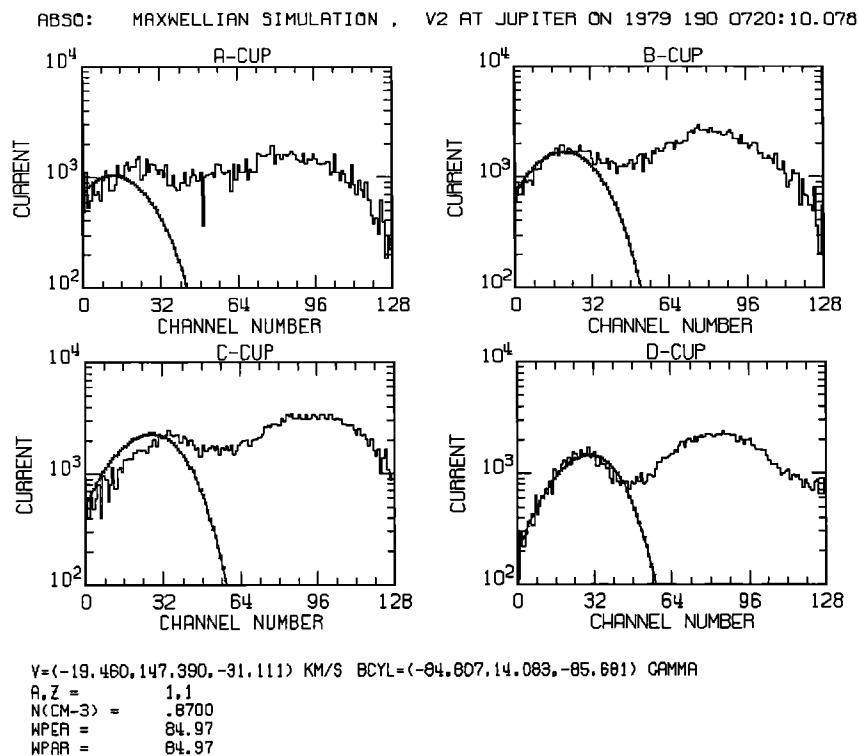


Fig. 8. Result of a fit to the spectra of Figure 7, assuming the ion distribution functions to be convected isotropic Maxwellians. The analysis is carried out for the protons only. Currents from all the cups could not be well simulated simultaneously.

that the largest nonazimuthal flows also tend to be the most field aligned. The ratio of the plasma flow along the magnetic field to the azimuthal flow is plotted against cylindrical radius (tilted dipole coordinates) in Figure 11. Parallel flow is seen to

contribute significantly to the overall plasma flow (azimuthal plus nonazimuthal) throughout the middle magnetosphere. Ratios of 0.2 and over are not uncommon. By contrast, the magnitude of the perpendicular flow component is much smaller. Figure 12

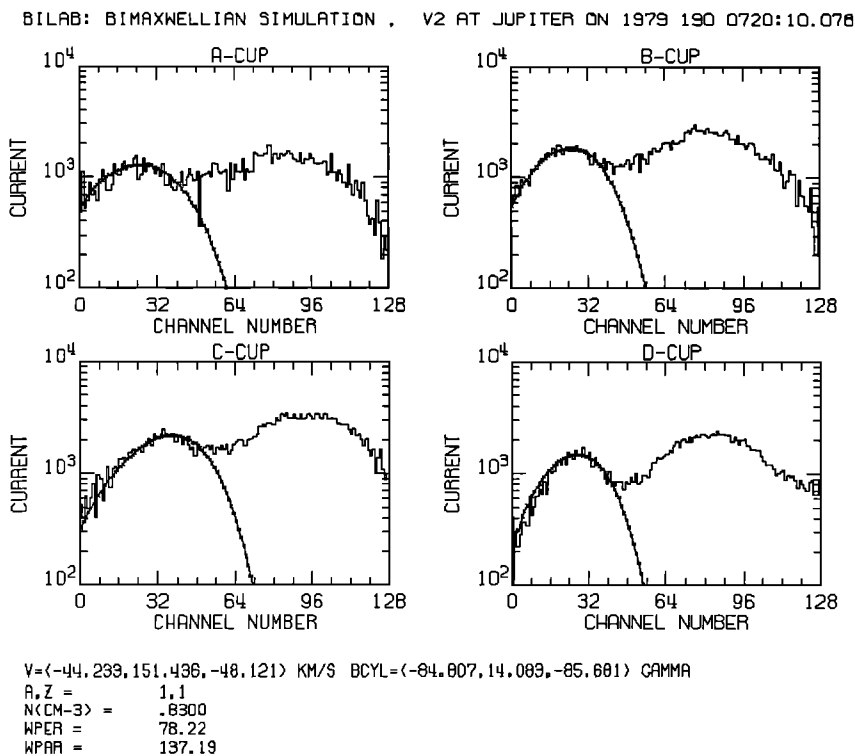


Fig. 9. Result of a fit to the spectrum of Figure 7, assuming the proton distribution function to be a bimaxwellian. Only the protons are fit, and, unlike those in the Maxwellian case, the currents from all four cups could be simulated.

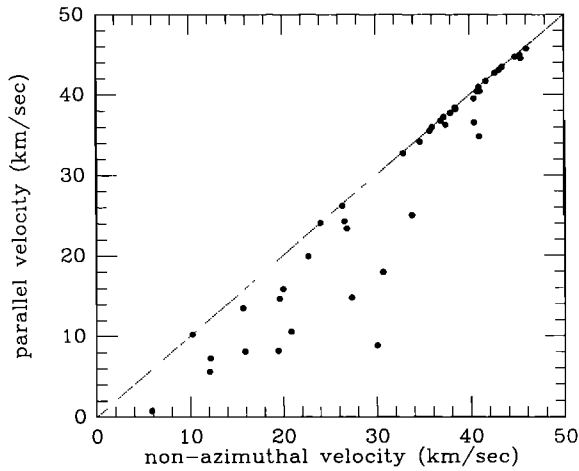


Fig. 10. Plasma flow along the magnetic field is plotted versus total nonazimuthal flow. Since parallel flow is contained within the nonazimuthal flow, V_{\parallel} can never exceed the magnitude of the nonazimuthal flow component; the dotted line represents this cutoff.

shows that the ratio of this component to the azimuthal flow never exceeds ~ 0.2 and averages only ~ 0.06 .

Radial transport of plasma through the magnetosphere can be inferred by considering the radial component of the cross-field flow, $V_{\perp r}$. The data show the occurrence of both inflow and outflow. For the most part, spectra during day 63 exhibit outflow, while during day 64 there is a substantial inflow. Time-dependent upstream solar wind conditions could account for this effect. During a period of increased solar wind ram pressure, the dayside magnetosphere would compress, giving rise to inward plasma flow. Subsequently, outflow would follow as the ram pressure decreased. McNutt *et al.* [1987] found by extrapolating measurements made upstream by Voyager 2 to Voyager 1 that the ram pressure was at a maximum on March 2 (day 61) and generally decreased afterward. Voyager was deep within the magnetosphere during day 64, so the effect of a decreased solar wind ram pressure may not have been "felt" yet (thus the inward flow), while further out, the magnetosphere was inflating owing to the decrease in ram pressure.

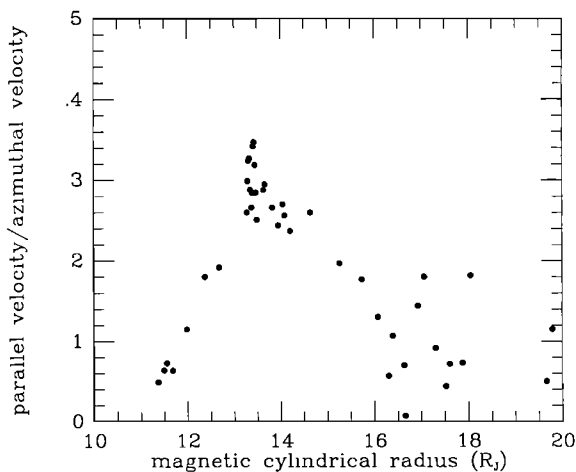


Fig. 11. Ratio between parallel plasma flow and azimuthal flow versus cylindrical radial distance. Parallel flow is seen to contribute significantly to the overall plasma flow (azimuthal plus nonazimuthal).

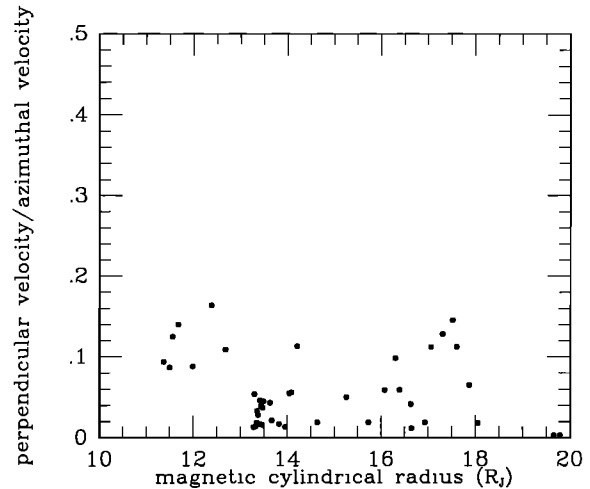


Fig. 12. Ratio between perpendicular plasma flow and azimuthal flow versus cylindrical radial distance. Perpendicular flow does not contribute significantly to the overall plasma flow (azimuthal plus nonazimuthal).

Implications for Corotating Convection

At Jupiter a convection system has been proposed by Hill *et al.* [1981] which would explain the Earth-based optical observations of a significant longitudinal asymmetry in the plasma torus associated with Io. This asymmetry is in the form of enhanced collisionally excited emission lines of singly ionized sulfur [Pücher and Morgan, 1980; Trauger *et al.*, 1980]. This convection system hinges on the magnetic anomaly in the northern hemisphere of Jupiter centered near the System III longitude $\lambda_{\text{III}} = 260^\circ$ [Acuña *et al.*, 1983].

The proposed convection system is fixed in the Jovian frame of reference because the magnetic anomaly, which drives the system, corotates with Jupiter. The region of the magnetosphere connected to this anomaly is known as the active sector, and spans about 100° in longitude centered near $\lambda_{\text{III}} = 225^\circ$ [Hill *et al.*, 1981; Vasyliunas and Dessler, 1981, and references therein].

Using plasma velocities obtained through this analysis, the corotating convection model for plasma transport can be directly tested. The plasma data which were analyzed cover a period of time during which the spacecraft traversed the active sector twice. The first crossing of the active sector began shortly after the spectral set on day 63 at 0841 SCET and ended before the spectral set on day 63 at 1527 SCET. The second traversal corresponds to the spectra acquired from day 63, 2103 SCET to day 64, 0025 SCET. No definite conclusion can be made about the radial outflow during the time of the first active sector crossing; no spectra were analyzed during this time owing to the lack of identifiable peaks and/or sufficient flux in at least three of the cups. Many spectra were analyzed during the second traversal of the active sector, however, and a survey of the results shows that both outflow and radial inflow occurred. Also, the spectra with the largest radial outflow (between day 63, 1819 SCET and 1903 SCET) do not lie within the active sector.

These results are contrary to those of Hairston and Hill [1985] (see also Hairston [1986]), who derived radial velocity components from magnetic field signatures and the basic MHD equations. Their cleanest results were obtained for the same three inbound magnetic equatorial crossings covered by the data used in this study. Table 1 lists the radial plasma flows obtained at each of the crossings and the corresponding values determined from this analysis. Crossings A and C are in the active sector with the

TABLE 1. Comparison of Radial Velocities

Crossing	Time, Day of Year, SCET	Time Range, Day of Year, SCET	<i>Hairston and Hill</i> [1985] Values Average Velocity, km/s Velocity Range, km/s	PLS Measurements	
				Average Velocity, km/s	Points in Range
A	63 1408	63 1201 to 63 1633	26.4 (17.4 – 35.2)	0.052 ± 0.38	2
B	63 1914	63 1754 to 63 2059	12.9 (9.1 – 15.0)	11.28 ± 7.08	12
C	64 0005	63 2154 to 64 0213	33.6 (22.5 – 47.9)	-2.18 ± 7.86	26

corresponding times listed. The sampling time interval for each crossing is also shown. The range of velocities obtained by *Hairston and Hill* [1985] are given in parentheses, while the preferred value is listed above them. For the two crossings inside the active sector the flows are radially outward and larger than the value obtained at crossing B (which is not within the active sector). The values quoted from this analysis were obtained by taking the values of V_{IR} and averaging them over the same range for each crossing (for the spectral sets with several fits, the value of the velocity component from the best fit was used). The average value obtained, standard deviation, and number of points used in computing the average are also shown. While the directly measured value from crossing B is consistent with those obtained from the analysis of the magnetic field data, the values from the

other two crossings clearly are not (although our determination for crossing A is probably not well determined; see discussion above).

During the outbound leg of the encounter, *Hairston and Hill* [1986] identified regions in which an inflow of supercorotating plasma is expected. This expectation is based upon the observed prograde spiral in the magnetic field lines [*Hairston*, 1986; *Hairston and Hill*, 1986]. Although almost all of the PLS spectra obtained outbound cannot be fully analyzed in an unambiguous way, there was one spectral set from which a velocity could be obtained. This set was obtained on day 64 at 1942 SCET at which time the spacecraft was $9.3 R_J$ from the planet and about $0.3 R_J$ below the magnetic equator; it is shown in Figure 13. When analyzed, this set did yield an inward radial flow

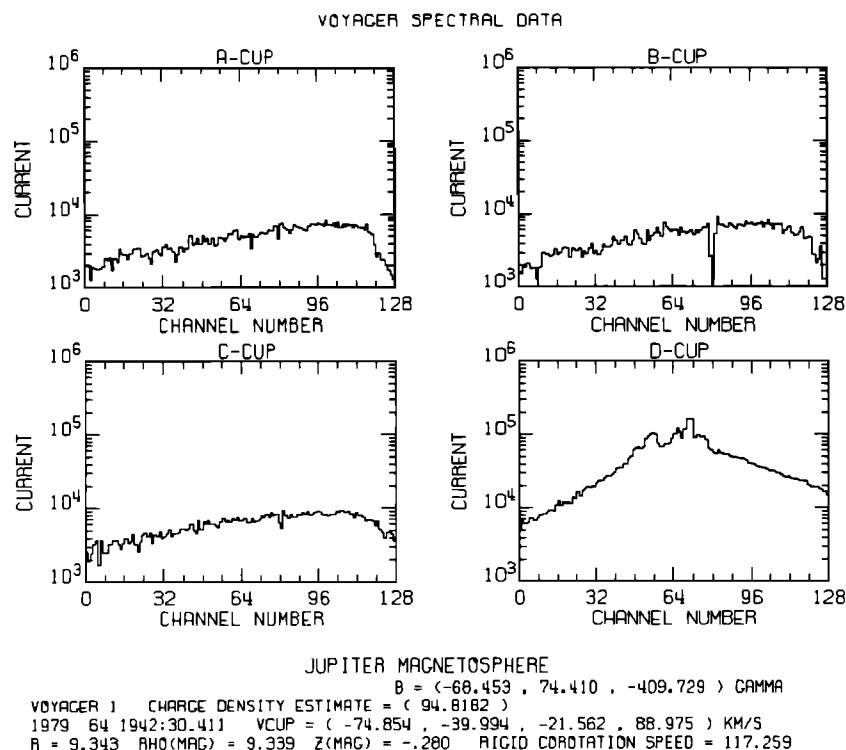


Fig. 13. A spectral set obtained on day 64 at 1942 SCET during the outbound leg of the Voyager 1 encounter with Jupiter. At this time the spacecraft was $9.3 R_J$ from the planet and about $0.3 R_J$ below the magnetic equator. This set is unique from the outbound pass in that resolved peaks are present in the D cup.

($V_R = -7.4$ km/s), however, the azimuthal velocity of $V_\phi = 115$ km/s is slightly less than the local corotational velocity of $V_\phi = 117$ km/s. This one set of spectra yields an azimuthal velocity component closer to corotation than those obtained at similar distances inbound; however, the plasma is not supercorotating. A hybrid model proposed by Hill *et al.* [1982] which combines corotating convection with radial diffusion, is also not consistent with the observed velocities. In this case the net mass transport is outward at all longitudes but larger in the active sector, and the azimuthal flow is subcorotational everywhere. Even though the problem of lack of supercorotation can be resolved in this fashion, the problem of observed plasma inflow remains. The latest version of the corotating convection model [Hill and Liu, 1987] can simulate the longitudinal mass symmetry associated with the line emissions from higher charge states of sulfur and oxygen in the outer torus [Brown *et al.*, 1983], but it still does not explain the observed inflow of the thermal plasma on the dayside.

The results of this analysis cast some doubt as to the validity of the corotating convection model as currently formulated and applied to the Jovian magnetosphere during the Voyager 1 flyby. At best, it would seem that if the convection model is valid, it is not an important part of the overall dynamical picture of the Jovian magnetosphere and may be radically disturbed by time-dependent changes produced by, e.g., the solar wind.

Consequences for Stress Balance

Jupiter is a rapid rotator, so, in a steady state situation, Newton's second law requires the inward Lorentz force from the current sheet to balance the outward component of the pressure gradient and centrifugal forces (as seen in a local rest frame). McNutt [1984] found, however, that the stresses did not match up; the Lorentz force was much too large. The magnetic field model used was a tilted dipole plus current sheet, which assumes an azimuthal current of strength $J = I_0/R$ flowing in an annulus of inner radius a , outer radius b , and half thickness D . The dimensions of the annulus as well as I_0 are parameters which are adjusted to optimal values by comparison with in situ magnetometer data [Connerney *et al.*, 1981].

Using a local modeling technique to determine the Lorentz stress as well as better estimates of the pressure gradient due to the hot plasma population, Mauk and Krimigis [1987] found that they could match up the particle and field stresses within $\sim 22 R_J$ of the planet. Outside of this distance they also found that there is a "missing" component to the particle-produced stress.

In these analyses the particle stresses were assumed to come from two sources: centrifugal force and pressure gradient force. The centrifugal force results primarily from the high-density "cold" plasma (detected by the PLS experiment), whereas the pressure gradient results primarily from the low-density "hot" plasma (detected by the Low Energy Charged Particle (LECP) experiment). This is simply a consequence of the plasma β ($\equiv 8\pi p/B^2$) for the "cold" plasma, being only a few percent, while the "hot" plasma β is often greater than 1 [McNutt, 1983; McNutt, 1984; Mauk and Krimigis, 1987]. The centrifugal force can be estimated the most reliably as it depends only upon local measurements. The outward centrifugal force density has a magnitude $\rho V_\phi^2/r$. Here the plasma mass density is given by ρ with r being the cylindrical radial distance from the spin axis of the system and V_ϕ the local azimuthal velocity component of the plasma (for the period considered, Voyager 1 moved from -1° to -2° in system III latitude, so r is effectively the radial distance from Jupiter). On the other hand, the pressure gradient must be

estimated from pressure values at several crossings of the (assumed) symmetry surface of the magnetic field [McNutt, 1983; McNutt, 1984; Mauk and Krimigis, 1987].

One possible explanation for the lack of agreement between inward and outward stresses is the neglect of possible field-aligned flows [McNutt, 1984; Mauk and Krimigis, 1987]. If field-aligned flow is assumed to exist, it will contribute to the outward stress in a manner similar to the azimuthal flow. The force density due to this parallel flow V_\parallel is $\rho V_\parallel^2/R_c$, where R_c is the local radius of curvature of the magnetic field line. A parallel component to the plasma flow is present, so the question of the extent to which field-aligned flow plays a role in the cross-field stress balance can be answered. Unfortunately, reliable, unambiguous results for the amount of field-aligned flow have been determined here only for distances within $20 R_J$ of Jupiter (with the exception of the single point in the vicinity of $25 R_J$ mentioned previously) where there is no major problem [Mauk and Krimigis, 1987]. Given the modeling inherent in the previous calculations of the Lorentz stresses, it is still relevant to consider possible contributions to stress balance due to field-aligned flows for the sake of checking consistency with the previous stress balance results.

We emphasize that this contribution to the balance of stresses from a field-aligned flow can be calculated directly from the data without making global assumptions about the magnetospheric geometry. Here, we carefully follow a procedure to minimize the assumptions folded into the data. The data suggest that $V_\parallel = 0$ at the symmetry plane of the magnetic field configuration near $17 R_J$; however, this does not hold near $13 R_J$ (cf. Figure 5). Only a nonzero flow at the (assumed) symmetry plane can contribute to the distension of the magnetic field such as that considered by McNutt, [1984]. On the other hand, flows away from this surface can contribute to a general "inflation" of the current sheet which would normally be associated only with pressure gradients. In what follows we determine quantitative contributions to both phenomena.

The radius of curvature R_c , and the magnetic field line curvature vector, κ , are given by

$$\frac{1}{R_c} \equiv |\kappa| \equiv |(\hat{\mathbf{b}} \cdot \nabla)\hat{\mathbf{b}}| \quad (1)$$

where $\hat{\mathbf{b}}$ is the magnetic field unit vector. By explicitly writing the unit vector $\hat{\mathbf{b}} = \mathbf{B}/B$ and using vector identities, (1) can be cast into the following form:

$$\kappa = \frac{4\pi}{c} \frac{\mathbf{J} \times \mathbf{B}}{B^2} + \nabla_\perp(\ln B) \quad (2)$$

where $\nabla_\perp \equiv \nabla - \hat{\mathbf{b}}(\hat{\mathbf{b}} \cdot \nabla)$. Using the current density profile obtained from the magnetic field model, the field curvature becomes

$$\kappa = \frac{4\pi I_0}{c} \frac{1}{RB^2} (B_R \hat{\mathbf{e}}_R - B_R \hat{\mathbf{e}}_z) + \nabla_\perp(\ln B) \quad (3)$$

The current density profile is valid for $|z| \leq 2.5 R_J$ and $5 R_J < R < 50 R_J$. From Connerney *et al.* [1981] a value of $4\pi I_0/c = 4.5 \times 10^{-3}$ G gives the best simulation of the observed field during the Voyager 1 encounter. Except for the $\nabla_\perp(\ln B)$ term and \mathbf{J} , all quantities are determined from in situ measurements. From Figure 5, at about $17.5 R_J$ and $14 R_J$, it can be seen that the spacecraft trajectory is approximately perpendicular to the magnetic field direction. Thus

$$\nabla_\perp(\ln B) \approx \frac{\Delta \ln B}{\Delta s} = \frac{\ln B_1 - \ln B_2}{\Delta s} \quad (4)$$

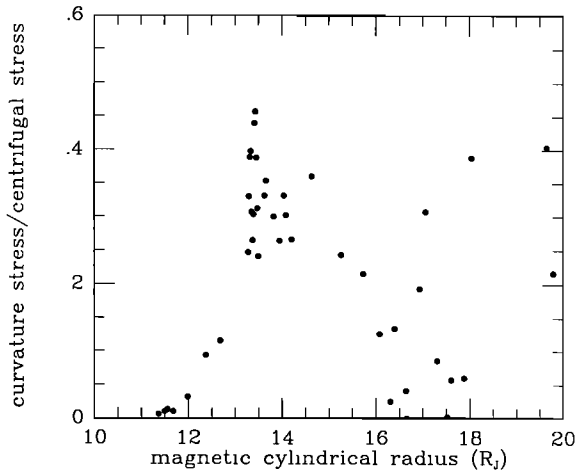


Fig. 14. Ratio of outward components of curvature to centrifugal stress versus magnetic cylindrical radius. The curvature term is seen to contribute as much as $\sim 45\%$ to the total stress due to the centrifugal force resulting from the azimuthal plasma flow.

where

$$\Delta s^2 \equiv (R_1 - R_2)^2 + (z_1 - z_2)^2 \quad (5)$$

which allows one to estimate $\nabla_{\perp}(\ln B)$ at a point, by knowing the spacecraft position (in magnetic cylindrical coordinates) and magnetic field on both sides of that point. The perpendicular gradient term was estimated for 10 spectra and added to the first term of (3) to calculate a radius of curvature. This value was then compared to the value of R_c which neglected the gradient contribution. For all cases, the effect of the $\nabla_{\perp}(\ln B)$ term is negligible. The largest contribution is associated with the spectrum at 1819 SCET on day 63, where $R_c = 2.18 R_J$ without the $\nabla_{\perp}(\ln B)$ piece and $R_c = 1.94 R_J$ with the added term (an 11% decrease in the size of R_c). All the other cases showed a decrease in the radius of curvature of less than 1%. Thus, neglecting $\nabla_{\perp}(\ln B)$ and substituting (3) into (1) gives

$$R_c \equiv \frac{1}{|\kappa|} \approx \frac{c}{4\pi I_0} RB \quad (6)$$

We have assumed that $B^2 = B_R^2 + B_z^2$ (i.e., $B_{\phi} = 0$). With the radius of curvature known, the ratio of the curvature stress to the centrifugal stress can be calculated. The component of the centrifugal force perpendicular to the field line is needed; hence, its projection into the $-\hat{\kappa}$ direction is required. The centrifugal force unit vector \hat{e}_c (the unit cylindrical radial vector with respect to the spin axis) can be written as

$$\hat{e}_c \approx \frac{R}{r} \hat{e}_R + \frac{z}{r} \hat{e}_z$$

where $r^2 = R^2 + z^2$ because the spacecraft lies in the rotational equatorial plane. Thus the ratio of the components of the two stresses in the $-\hat{\kappa}$ direction is

$$f = \frac{V_{\parallel}^2}{R_c} \frac{r}{V_{\phi}^2 \delta} \quad (7)$$

where

$$\delta \equiv -\hat{\kappa} \cdot \hat{e}_c \quad (8)$$

with $\hat{\kappa}$ a unit vector in the direction of κ ; δ is known because $\hat{\kappa}$ can be determined using (3) and (4).

A plot of f versus magnetic cylindrical radius is shown in Figure 14. The curvature stress generally contributes 20 – 50% to the total inertial stress, a significant contribution. However, the contributions at the two crossings of the magnetic equatorial plane are still small compared to the centrifugal stress.

The isolated point at $25 R_J$ is located only $0.22 R_J$ below the nominal magnetic equator, yet the parallel velocity component is high, ~ 68 km/s, as mentioned above. If the inferred radius of curvature of $\sim 1.23 R_J$ is correct, then the ratio of curvature to centrifugal stress for this point is ~ 3.0 . On the basis of this one point, it is not possible to conclude that field-aligned streaming is the source of the missing particle stress; indeed this relatively large value would appear not to be large enough to satisfy the balance condition near $\sim 30 R_J$ [Mauk and Krimigis, 1987]. However, this one analyzed point does keep open the latter possibility. As modeling efforts on the plasma data from Jupiter continue, more work will be done in this region in an attempt to at least set some limits on this effect. In passing, it should be noted that in the region covered by this analysis, bidirectional flows and "missed flows" near the magnetic equator can be ruled out; outside this region more work must be done to assess the limits that can be placed on flow parameters versus viewing angle limitations of the PLS sensors. More progress may be possible; the situation is not as hopeless as suggested by Mauk and Krimigis [1987].

As Mauk and Krimigis [1987] point out, an exact balance may not occur owing to the dynamical effects of radial transport of plasma. In addition, time-dependent effects could also have a significant effect. On the other hand, it is disquieting that the apparent discrepancy is as large as it is without some other obvious signature in the fields and particles data. In the region covered by this analysis we have shown that the observed field-aligned (antialigned) flows are not responsible for a significant contribution to the radial distension of the magnetosphere; however, they do contribute to the inflation of the magnetosphere perpendicular to the symmetry plane in this region. A full assessment of this latter effect requires a detailed comparison with inferred hot plasma gradients off the equator and is beyond the scope of this study.

SUMMARY

An in-depth study of the plasma data obtained from the Voyager 1 spacecraft encounter with Jupiter has been performed. The knowledge and use of the full response function of the Plasma Science experiment has made accurate determination of plasma bulk flow velocities possible in the middle magnetosphere of Jupiter. The first result of this analysis is the reconfirmation of subcorotational plasma flow. However, the major result is the confirmation and quantification of the substantial nonazimuthal component of the plasma flow. The magnitude of this component is as large as $\sim 40\%$ of the local azimuthal speed, with 20% a typical value. Resolving the nonazimuthal flow into parallel and perpendicular components (with respect to the magnetic field) shows that most of the flow is field-aligned (anti-field-aligned). On the dayside in much of the region treated, plasma above the magnetic equator moves in an anti-field-aligned direction, while below the equator, plasma tends to move in a field-aligned direction, i.e., away from the magnetic equator. This result is similar to that found at much higher energies during the Pioneer 10 encounter with Jupiter.

The cross-field component of the bulk plasma motion exhibits both inflow and outflow. This result is very interesting in that the presumed dominance of Jupiter's rotation on magnetospheric

motion at these distances combined with the plasma output of Io suggests that, to lowest order, the system is azimuthally symmetric in this region, further implying that only outflow of plasma would be observed. A modification to this simple picture by the corotating convection model can also be ruled out (see, e.g., *Vasyliunas* [1983] and *Hill et al.* [1983]).

To obtain all the components of the convective velocity, a nonlinear least squares analysis was performed. Assuming the ion distribution function to be a convected Maxwellian, a plasma velocity is calculated which is consistent with the data. However, these derived velocities could, in principle, depend upon the thermal anisotropy if the latter is large enough. The viewing geometry of the instrument is such that most of the observed signal is due to flow and/or plasma temperature perpendicular to the magnetic field. However, the B and C cups also sample, to a lesser extent, field-aligned flow and/or plasma temperature along the field lines. Thus a large thermal anisotropy is required for it to be "seen" by the PLS instrument. To quantify this effect, we developed an analysis algorithm which uses the full response function of the instrument and allows the model ion distribution function to be a convected bimaxwellian. Several spectra were then reanalyzed and the results compared to the simulations, assuming a Maxwellian distribution. The assumption of bimaxwellian versus Maxwellian distribution is found to have little effect on the velocity determinations. In fact, none of the spectra analyzed from the Voyager 1 encounter show a unique signature of a thermal anisotropy. A temperature anisotropy is fairly independent of the flow for the spectra considered, and convected Maxwellians simulate the measured currents quite well.

A set of spectra from the Voyager 2 encounter with Jupiter was analyzed by assuming both a Maxwellian and a bimaxwellian ion distribution function. This set could only be simulated if a convected bimaxwellian distribution is assumed for the ions. Both a significant thermal anisotropy ($T_{\parallel}/T_{\perp} = 3.08$) and nonazimuthal flow were deduced.

The derived plasma velocities were used to investigate their implications for plasma transport and stress balance. One model of plasma transport hypothesizes that a localized depression of the surface magnetic field strength of Jupiter enhances radially outward plasma flow (corotating convection model) for a particular range of longitudes [*Hill et al.*, 1981]. The plasma data analyzed covered a period of time during which Voyager went through the associated active sector twice. Examination of the velocities showed no such enhanced flow inside the active sector. In fact, during one traversal most of the radial flow was inward, not outward (as required by this model). *Hairston and Hill* [1986] have suggested that supercorotational flow was present on the nightside of Jupiter during the Voyager 1 encounter, supporting the corotating convection hypothesis. However, the analyzed spectral set from this region shows no significant departure from corotation in either a subcorotational or supercorotational sense. The results of the analysis cast some doubt as to the validity of the corotating convection model, at least as currently formulated, and possibly introduce a problem in reconciling the plasma and magnetic signatures during some of the current sheet crossings. At best, it appears that if the corotating convection model is valid, it was not an overriding part of the overall dynamical picture of the Jovian magnetosphere at the epoch of the Voyager 1 encounter.

Using the currently accepted magnetic field model of the Jovian magnetosphere, a stress balance analysis can be performed. Assuming the magnetosphere is in equilibrium, the sum total of

the stresses should be zero. However, the inwardly directed $\mathbf{J} \times \mathbf{B}$ force from the model is much larger than the outwardly directed centrifugal and pressure gradient forces in some regions. The plasma flow exhibits a large field-aligned component, so a stress due to magnetic field line curvature must be considered. By calculating the radius of curvature of the magnetic field (at the point of observation) and using V_{\parallel} , the relative importance of curvature stress to the overall missing stress can be ascertained. In most of the region of the Jovian magnetosphere investigated in this study the force imbalance is not serious. The curvature stress can be as large as 50% of the usual centrifugal stress from azimuthal flow, and the additional outward stress is sufficiently small not to be in conflict with approximate balance in this region [*McNutt*, 1984; *Mauk and Krimigis*, 1987]. One point investigated suggests a larger contribution to the stress by field-aligned flow, but the nature of the apparently missing outward stress remains a mystery.

APPENDIX

Current measured by the PLS experiment, for a given energy-per-charge channel k , is given by the relation

$$I_k(\mathbf{x}, t) = \bar{I}_k^+(\mathbf{x}, t) - \bar{I}_{k+1}^-(\mathbf{x}, t) \quad (\text{A1})$$

where $\bar{I}_k^+(\mathbf{x}, t)$ and $\bar{I}_{k+1}^-(\mathbf{x}, t)$ are the total currents measured by the instrument (at location \mathbf{x} and time t) due to positive ions with velocities greater than the threshold velocities for channels k and $k+1$, respectively. These threshold velocities are defined by

$$v_k \equiv \left[\frac{2eZ_i^+ \phi_k}{A_i m_p} \right]^{1/2} \quad (\text{A2})$$

with e and m_p being the proton charge and mass, respectively. For ionic species i the mass number and charge state are denoted by A_i and Z_i^+ , respectively. The set of contiguous potentials provided by the modulator grid of a given Faraday cup to select the energy-per-charge channels is ϕ_k , where k goes from 1 to N and N is 16 for the L mode and 128 for the M mode [see *Bridge et al.*, 1977]. Thus the current measured for the k th channel is principally due to particles with velocities which fall into the velocity window of width Δv_k , where

$$\Delta v_k = v_{k+1} - v_k \quad (\text{A3})$$

although particles outside of this range can also contribute significantly due to the nature of the response discussed below. This extra contribution constitutes the "feedthrough" current.

The total measured currents making up the terms on the right hand side of (A1) are given by

$$\bar{I}_k^+(\mathbf{x}, t) = Ze \int_{-\infty}^{\infty} \int_{-\infty}^{\infty} \int_{v_k}^{\infty} d\mathbf{v} (\mathbf{v} \cdot \hat{\mathbf{n}}) f(\mathbf{x}, \mathbf{v}, t) R(\mathbf{v}, v_k) \quad (\text{A4})$$

where $\hat{\mathbf{n}}$ is a unit vector in the direction normal to the PLS cup being considered. Thus

$$\bar{I}_k^-(\mathbf{x}, t) = Ze \int_{-\infty}^{\infty} dv_x \int_{-\infty}^{\infty} dv_y \int_{v_k}^{\infty} dv_z v_z f(\mathbf{x}, \mathbf{v}, t) R(\mathbf{v}, v_k) \quad (\text{A5})$$

where $f(\mathbf{x}, \mathbf{v}, t)$ is the ion distribution function and $R(\mathbf{v}, v_k)$ is defined as the instrument response function and is analyzed in great detail by *Barnett* [1984] and *Barnett and Olbert* [1986]. Symbolically, $R(\mathbf{v}, v_k)$ can be written as a product of two terms,

$$R(\mathbf{v}, \nu_k) = T(\mathbf{v}, \nu_k) A(\mathbf{v}, \nu_k) \quad (\text{A6}) \quad \text{with}$$

where $T(\mathbf{v}, \nu_k)$ is defined as the transparency function and $A(\mathbf{v}, \nu_k)$ the "sensitive" area of the collector.

The transparency of a given grid within the cup is defined as the probability of an incident particle passing, unobstructed, through the grid plane. Since each cup of the main sensor has nine such grids, $T(\mathbf{v}, \nu_k)$ is a product of the nine associated probabilities; the side sensor has eight grids, hence, eight such probabilities. This final probability can be parameterized in terms of four gaussians [Barnett, 1984; Barnett and Olbert, 1986]. The sensitive area is defined to be the area overlap of the collector with the projected image of the aperture onto the collector. The product of the transparency function and sensitive area, at normal incidence, is defined as the effective area, where $A_0 T_0 = 67.3 \text{ cm}^2$ for each of the three cups making up the main sensor and $A_0 T_0 = 56.2 \text{ cm}^2$ for the side sensor.

To completely specify the currents $I_k^*(\mathbf{x}, t)$, we must specify an analytic form of the distribution function of the ions, $f(\mathbf{x}, \mathbf{v}, t)$. Two different ion distributions have been used to explicitly evaluate (A5): a convected isotropic Maxwellian distribution and a convected bimaxwellian distribution. The case of a convected isotropic Maxwellian distribution is covered by Barnett [1984] for all four cups of the PLS instrument. The bimaxwellian case is discussed below.

In general, a bimaxwellian distribution function can be written in the following form (see, e.g., Rossi and Olbert [1970]),

$$f(\mathbf{x}, \mathbf{v}, t) = \frac{n}{\pi^{3/2} w_{\parallel} w_{\perp}^2} \exp \left\{ -\frac{|\mathbf{v} - \mathbf{u}|^2}{w_{\perp}^2} - \left[\frac{1}{w_{\parallel}^2} - \frac{1}{w_{\perp}^2} \right] |(\mathbf{v} - \mathbf{u}) \cdot \hat{\mathbf{b}}|^2 \right\} \quad (\text{A7})$$

where

$w_{\parallel}(\mathbf{x}, t) \equiv$ ion parallel thermal speed

$w_{\perp}(\mathbf{x}, t) \equiv$ ion perpendicular thermal speed

$\mathbf{u}(\mathbf{x}, t) \equiv$ ion bulk velocity

$\hat{\mathbf{b}}(\mathbf{x}, t) \equiv$ magnetic field unit vector

$n(\mathbf{x}, t) \equiv$ ion number density

$\mathbf{v} \equiv$ particle velocity

Inserting the above expression of $f(\mathbf{x}, \mathbf{v}, t)$ into (A5) and knowing the response function yields for the total current,

$$I_k^* = \frac{1}{s^2} \sum_{i,j=1}^2 B_{ij} \int_{\nu_k} d\nu_x \nu_x^2 I_x \int_{-\infty}^{\infty} dX I_x(X) \int_{-\infty}^{\infty} dY I_y(X, Y) \quad (\text{A8})$$

where

$$\begin{aligned} I_x(X) &\equiv \exp(-\beta_x X^2 + 2\gamma_x X) A_x \\ I_y(X, Y) &\equiv \exp[-\beta_y Y^2 + 2\gamma_y(X)Y] A_y \\ I_z &\equiv \exp(-\beta_z \nu_z^2 + 2\gamma_z \nu_z) \end{aligned} \quad (\text{A9})$$

$$\beta_x \equiv \left[\frac{\nu_x}{s} \right]^2 \left[\frac{1}{w_{\parallel}^2} + \left[\frac{1}{w_{\parallel}^2} - \frac{1}{w_{\perp}^2} \right] b_x^2 + \frac{a_1}{\nu_x^2} \right]$$

$$\beta_y \equiv \left[\frac{\nu_y}{s} \right]^2 \left[\frac{1}{w_{\parallel}^2} + \left[\frac{1}{w_{\parallel}^2} - \frac{1}{w_{\perp}^2} \right] b_y^2 + \frac{a_2}{\nu_y^2} \right]$$

$$\beta_z \equiv \frac{1}{w_{\parallel}^2} + \left[\frac{1}{w_{\parallel}^2} - \frac{1}{w_{\perp}^2} \right] b_z^2$$

(A10)

$$\gamma_x \equiv \left[\frac{\nu_x}{s} \right] \left\{ \frac{u_x}{w_{\parallel}^2} - \left[\frac{1}{w_{\parallel}^2} - \frac{1}{w_{\perp}^2} \right] b_x \left[\nu_x b_x - (\mathbf{u} \cdot \hat{\mathbf{b}}) \right] \right\}$$

$$\gamma_y(X) \equiv \left[\frac{\nu_y}{s} \right] \left\{ \frac{u_y}{w_{\parallel}^2} - \left[\frac{1}{w_{\parallel}^2} - \frac{1}{w_{\perp}^2} \right] b_y \left[\left[\frac{X \nu_x}{s} \right] b_x + \nu_x b_x - (\mathbf{u} \cdot \hat{\mathbf{b}}) \right] \right\}$$

$$\gamma_z \equiv \frac{u_z}{w_{\parallel}^2} + \left[\frac{1}{w_{\parallel}^2} - \frac{1}{w_{\perp}^2} \right] b_z (\mathbf{u} \cdot \hat{\mathbf{b}})$$

and

$$B_{ij}(\mathbf{x}, t) \equiv \frac{Z^* e n T_0 A_0}{\pi^{3/2} w_{\parallel} w_{\perp}^2} c_i c_j$$

$$\times \exp \left\{ -\left[\frac{u^2}{w_{\perp}^2} + \left[\frac{1}{w_{\parallel}^2} - \frac{1}{w_{\perp}^2} \right] (\mathbf{u} \cdot \hat{\mathbf{b}})^2 \right] \right\}$$

The x and y components of the sensitive area are denoted by A_x and A_y , respectively [Barnett and Olbert, 1986], while the variables of integration, X and Y , are defined in the following manner

$$X \equiv \left[\frac{\nu_x}{\nu_z} \right] s \quad Y \equiv \left[\frac{\nu_y}{\nu_z} \right] s \quad (\text{A11})$$

The shift function s is defined by

$$\mathbf{s}^* = s \left[\frac{\mathbf{v}}{\nu_z} \right] h \quad (\text{A12})$$

where h is the distance between the aperture and collector and \mathbf{s}^* is the shift vector. This shift vector is then defined as the displacement of the aperture image from a perpendicular projection of the aperture onto the plane of the collector. This shift results from the refraction of the ion trajectory within the instrument due to the electric fields between the various grids. In practice, s is a complicated function of the modulator and suppressor voltages and is stored in tabular form. Finally, the constants a_1 , a_2 , c_1 , and c_2 are used in the parameterized expression of the transparency function; they were found from fitting the true transparency function to the sum of two gaussians and are also stored in tabular form for doing computations [Barnett and Olbert, 1986].

A nonzero temperature anisotropy shows up via the expression $(w_{\parallel}^2 - w_{\perp}^2)$. This factor can dominate terms in the expressions which contain it. This temperature anisotropy factor greatly increases the mathematical complexity required to evaluate the model currents. This occurs because γ has an X dependence

which adds considerable analytical complexity over the Maxwellian case.

Since there is an X dependence in the integrand of the Y integral, we evaluate the latter integral first. Looking only at the Y integral in (A8) and completing the square in the exponential term in I_y , we obtain

$$K(X) \equiv \int_{-\infty}^{\infty} dY I_y(X, Y) = \frac{1}{\beta_y^{3/2}} \exp\left[\frac{\gamma_y^2(X)}{\beta_y}\right] \int_{-\infty}^{\infty} dZ A_y e^{-Z^2} \quad (\text{A13})$$

where

$$Z \equiv \beta_y^{1/2} \left[Y - \frac{\gamma_y(X)}{\beta_y} \right] \quad (\text{A14})$$

and upon integrating, gives

$$K(X) = \frac{1}{2} \left[\frac{\pi}{\beta_y} \right]^{1/2} \exp\left[\frac{\gamma_y^2(X)}{\beta_y}\right] \times \left[\frac{\phi(Z_u) - \phi(Z_w)}{Z_u - Z_w} - \frac{\phi(Z_d) - \phi(Z_a)}{Z_d - Z_a} \right] \quad (\text{A15})$$

with

$$\phi(Z) \equiv Z \operatorname{erf}(Z) + \frac{1}{\sqrt{\pi}} e^{-Z^2} \quad (\text{A16})$$

and $\operatorname{erf}(Z)$ being the error function, namely,

$$\operatorname{erf}(Z) \equiv \frac{2}{\sqrt{\pi}} \int_0^Z e^{-t^2} dt$$

The subscripts on Z in (A15) refer to constants which are values of Y corresponding to five contiguous ranges over which different parameterized expressions of the sensitive area are used in the integral of (A13). This departs somewhat from the treatment of *Barnett and Olbert* [1986], who retain an X dependence of these values of Y . Weighted constants must be used here owing to the difficulties introduced into the next integration by the anisotropy. Details of the differences are given by *Sands* [1987].

To obtain an analytical solution of the X integral (defined as $G(v_z)$), the function $\phi(Z)$ must be fit to a set of elementary functions. The empirical relation for $\phi(Z)$ is

$$\phi(Z) \approx |Z| + \frac{1}{\sqrt{\pi}} e^{-Z^2} + |Z| \left[c_1 e^{-a_1 Z^2} + c_2 e^{-a_2 Z^2} \right] \quad (\text{A17})$$

where

$$\begin{aligned} a_1 &= 1.3 \\ a_2 &= 7.0 \\ c_1 &= -0.6 \\ c_2 &= -0.3 \end{aligned}$$

with a maximum error of $\sim 0.2\%$ occurring in the interval $Z = 0.0$ to $Z = 2.5$. Since the X dependence in Z_u and Z_d is weak (see above), it is neglected, and the integration can be performed analytically. After quite a bit of algebra, $G(v_z)$ becomes

$$G(v_z) = \frac{g_u(v_z) - g_w(v_z)}{Z_u - Z_w} - \frac{g_d(v_z) - g_a(v_z)}{Z_d - Z_a} \quad (\text{A18})$$

Subscripts on the g functions indicate which Y is being used. The function g is a very complicated function of v_z and can have one of 10 possible forms (these are given by *Sands* [1987]). This complexity is a result of the facts that the empirical approximation of $\phi(Z)$ is a function of $|Z|$ and the sensitive area has been parameterized.

The total current can then be written as

$$\begin{aligned} I_k^r &= \frac{1}{s^2} \sum_{i,j=1}^2 B_{ij} \int_{v_k}^{\infty} dv_z v_z^3 G(v_z) \quad (\text{A19}) \\ &\times \exp \left\{ -v_z^2 \left[\frac{1}{w_{\parallel}^2} + \left[\frac{1}{w_{\parallel}^2} - \frac{1}{w_{\perp}^2} \right] b_z^2 \right] \right. \\ &\left. + 2v_z \left[\frac{u_z}{w_{\parallel}^2} + \left[\frac{1}{w_{\parallel}^2} - \frac{1}{w_{\perp}^2} \right] b_z (\mathbf{u} \cdot \hat{\mathbf{b}}) \right] \right\} \end{aligned}$$

The final integration over v_z in (A19), must be done numerically. The integrand is so convoluted that no analytical solution is possible unless many assumptions are made which result in a serious limitation to the usefulness of the analysis. Once $I_k^r(\mathbf{x}, t)$ is found numerically, the current measured in any given channel k , due to a given set of plasma parameters, can be calculated using (A1).

Acknowledgments. The authors thank H. S. Bridge and J. W. Belcher for access to the plasma data and for their support over the course of this study. They thank T. G. Northrop for pointing out further published work on the field-aligned streaming of high-energy particles measured by Pioneer 10. They also thank J. D. Richardson and the referees for helpful comments and N. F. Ness for access to the Voyager magnetic field data. This work was supported by NASA under contracts 953733 and 957781 from the Jet Propulsion Laboratory to the Massachusetts Institute of Technology.

The Editor thanks A. Nishida and another referee for their assistance in evaluating this paper.

REFERENCES

- Acuña, M. H., K. W. Behannon, and J. E. P. Connerney, Jupiter's magnetic field and magnetosphere, in *Physics of the Jovian Magnetosphere*, edited A. J. Dessler, chap. 1, Cambridge University Press, New York, 1983.
- Barnett, A., *Tech. Rep. CSR-TR-84-1*, The response function of the Voyager plasma science experiment, Mass. Inst. of Tech. Cent. for Space Res., Cambridge, 1984.
- Barnett, A., In situ measurements of the plasma bulk velocity near the Io flux tube, *J. Geophys. Res.*, **91**, 3011, 1986.
- Barnett, A., and S. Olbert, The response function of modulator grid Faraday cup plasma instruments, *Rev. Sci. Instr.*, **57** (10), 2432, 1986.
- Belcher, J. W., and R. L. McNutt, Jr., The dynamic expansion and contraction of the Jovian plasma sheet, *Nature*, **287**, 813, 1980.
- Belcher, J. W., C. K. Goertz, and H. S. Bridge, The low energy plasma in the Jovian magnetosphere, *Geophys. Res. Lett.*, **7**, 17, 1980.
- Bevington, P. S., *Data Reduction and Error Analysis for the Physical Sciences*, McGraw-Hill, New York, 1969.
- Bridge, H. S., J. W. Belcher, R. J. Butler, A. J. Lazarus, A. M. Mavretic, J. D. Sullivan, G. L. Siscoe, and V. M. Vasyliunas, The plasma experiment on the 1977 Voyager mission, *Space Sci. Rev.*, **21**, 259, 1977.

- Bridge, H. S., et al., Plasma observations near Jupiter: Initial results from Voyager 1, *Science*, **204**, 987, 1979a.
- Bridge, H. S., et al., Plasma observations near Jupiter: Initial results from Voyager 2, *Science* **206**, 972, 1979b.
- Brown, D. C., D. C. Hamilton, G. Gloeckler, Azimuthal flow speed of energetic ions in the Jovian dayside magnetosphere, *Eos Trans. AGU*, **66**, 1048, 1985.
- Brown, R. A., Observed departure of the Io plasma torus from rigid corotation with Jupiter, *Astrophys. J.*, **268**, L47, 1983.
- Brown, R. A., C. B. Pilcher, and D. F. Strobel, Spectrophotometric studies of the Io torus, in *Physics of the Jovian Magnetosphere*, edited A. J. Dessler, chap. 6, Cambridge University Press, New York, 1983.
- Carbary, J. F., S. M. Krimigis, E. P. Keath, G. Gloeckler, W. I. Axford, and T. P. Armstrong, Ion anisotropies in the outer Jovian magnetosphere, *J. Geophys. Res.*, **86**, 8285, 1981.
- Connerney, J. E. P., M. H. Acuña, and N. F. Ness, Modeling the Jovian current sheet and inner magnetosphere, *J. Geophys. Res.*, **86**, 8370, 1981.
- Hairston, M. R., Plasma outflow and superrotation in the Jovian magnetosphere deduced from Voyager observations, Ph.D. thesis, Dept. of Space Phys. and Astron., Rice Univ., Houston, Tex., 1986.
- Hairston, M. R., and T. W. Hill, Jovian ionospheric conductivity and magnetospheric plasma outflow: Voyager 1, *J. Geophys. Res.*, **90**, 9889, 1985.
- Hairston, M. R., and T. W. Hill, Superrotation in the pre-dawn Jovian magnetosphere: Evidence for corotating convection, *Geophys. Res. Lett.*, **13**, 521, 1986.
- Hill, T. W., Inertial limit on corotation, *J. Geophys. Res.*, **84**, 6554, 1979.
- Hill, T. W., Corotation lag in Jupiter's magnetosphere: Comparison of observation and theory, *Science*, **207**, 301, 1980.
- Hill, T. W., and W. W. Liu, Corotating convection revisited, *Geophys. Res. Lett.*, **14**, 178, 1987.
- Hill, T. W., A. J. Dessler, and L. J. Maher, Corotating magnetospheric convection, *J. Geophys. Res.*, **86**, 9020, 1981.
- Hill, T. W., C. K. Goertz, and M. F. Thomsen, Some consequences of corotating magnetospheric convection, *J. Geophys. Res.*, **87**, 8311, 1982.
- Hill, T. W., A. J. Dessler, and C. K. Goertz, Magnetospheric models, in *Physics of the Jovian Magnetosphere*, edited by A. J. Dessler, chap. 10, Cambridge University Press, New York, 1983.
- Mauk, B. H., and S. M. Krimigis, Radial force balance within Jupiter's dayside magnetosphere, *J. Geophys. Res.*, **92**, 9931, 1987.
- McDonald, F. B., A. W. Schardt, and J. H. Trainor, Energetic protons in the Jovian magnetosphere, *J. Geophys. Res.*, **84**, 2579, 1979.
- McNutt, R. L., Jr., Force balance in the magnetospheres of Jupiter and Saturn, *Adv. Space Res.*, **3**, 55, 1983.
- McNutt, R. L., Jr., Force balance in outer planet magnetospheres, *SPI Conference Proceedings and Reprint Series*, vol. 5, p.179, Scientific Publishers, Cambridge, Mass, 1984.
- McNutt, R. L., Jr., J. W. Belcher, J. D. Sullivan, F. Bagenal, and H. S. Bridge, Departure from rigid corotation of plasma in Jupiter's dayside magnetosphere, *Nature*, **280**, 803, 1979.
- McNutt, R. L., Jr., J. W. Belcher, and H. S. Bridge, Positive ion observations in the middle magnetosphere of Jupiter, *J. Geophys. Res.*, **86**, 8319, 1981.
- McNutt, R. L., Jr., P. S. Coppi, R. S. Selesnick, and B. Coppi, Plasma depletions in the Jovian magnetosphere: Evidence of transport and solar wind interaction, *J. Geophys. Res.*, **92**, 4377, 1987.
- Northrop, T. G., Residence lifetimes of 1.79- to 2.15-MeV protons in the equatorial region of the Jovian magnetosphere, *J. Geophys. Res.*, **84**, 5813, 1979.
- Northrop, T. G., and A. W. Schardt, Instability of equatorial protons in Jupiter's mid-magnetosphere, *J. Geophys. Res.*, **85**, 25, 1980.
- Northrop, T. G., C. K. Goertz, and M. F. Thomsen, The magnetosphere of Jupiter as observed with Pioneer 10, 2. Nonrigid rotation of the magnetodisc, *J. Geophys. Res.*, **79**, 3579, 1974.
- Northrop, T. G., T. J. Birmingham, and A. W. Schardt, Anisotropies in the fluxes of Pioneer 10 protons, *J. Geophys. Res.*, **84**, 47, 1979.
- Paonessa, M., Corotation anisotropies of energetic ions in Jupiter's magnetosphere, *Eos Trans. AGU*, **66**, 1048, 1985.
- Pilcher, C. B., and J. S. Morgan, The distribution of [SII] emission around Jupiter, *Astrophys. J.*, **238**, 375, 1980.
- Pontius, D. H., Jr., T. W. Hill, and M. E. Rassbach, Steady state plasma transport in a corotation dominated magnetosphere, *Geophys. Res. Lett.*, **11**, 1097, 1986.
- Rossi, B., and S. Olbert, *Introduction to the Physics of Space*, McGraw-Hill, New York, 1970.
- Sands, M. R., Structure of Jupiter's dayside middle magnetosphere, Ph.D. thesis, Nucl. Eng. Dep. and Cent. for Space Res., Mass. Inst. of Technol., Cambridge, 1987.
- Sittler, E. C., and D. F. Strobel, Io plasma torus electrons: Voyager 1, *J. Geophys. Res.*, **92**, 5741, 1987.
- Smith, E. J., L. Davis, Jr., D. E. Jones, P. J. Coleman, Jr., D. S. Colburn, P. Dyal, and C. P. Sonett, Jupiter's magnetic field, magnetosphere, and interaction with the solar wind: Pioneer 11, *Science*, **188**, 451, 1975.
- Trauger, J. T., G. Munch, and F. L. Roesler, A study of the Jovian [SII] nebula at high spectral resolution, *Astrophys. J.*, **236**, 1035, 1980.
- Van Allen, J. A., D. N. Baker, B. A. Randall, and D. D. Sentman, The magnetosphere of Jupiter as observed with Pioneer 10, 1. Instrument and principle findings, *J. Geophys. Res.*, **79**, 3559, 1974.
- Vasyliunas, V. M., Plasma distribution and flow, in *Physics of the Jovian Magnetosphere*, edited by A. J. Dessler, chap. 11, Cambridge University Press, New York, 1983.
- Vasyliunas, V. M., and A. J. Dessler, The magnetic-anomaly model of the Jovian magnetosphere: A post-Voyager assessment, *J. Geophys. Res.*, **86**, 8435, 1981.

R. L. McNutt, Jr., Massachusetts Institute of Technology, Room 37-635, Cambridge, MA 02139.

M. R. Sands, Science Applications International Corporation, 1710 Goodridge Dr., Mailstop G-8-1, McLean, VA 22102.

(Received August 6, 1987;
revised April 5, 1988;
accepted April 19, 1988.)